ELSEVIER

Nuclear Physics A 627 (1997) 222–238

NUCLEAR PHYSICS A

Single neutron emission following ^{11}Li β-decay

D.J. Morrissey [a,c], K.N. McDonald [a,c,1], D. Bazin [c], B.A. Brown [b,c], R. Harkewicz [a,c], N.A. Orr [c,2], B.M. Sherrill [b,c], G.A. Souliotis [a,c,3], M. Steiner [b,c], J.A. Winger [c,4], S.J. Yennello [c,5], B.M. Young [b,c,6] S. Lukyanov [d], G. Chubarian [d,5], Yu.Ts. Oganessian [d]

[a] *Department of Chemistry, Michigan State University, E. Lansing, MI 48824, USA*
[b] *Department of Physics and Astronomy, Michigan State University, E. Lansing, MI 48824, USA*
[c] *National Superconducting Cyclotron Laboratory, Michigan State University, E. Lansing, MI 48824, USA*
[d] *Laboratory of Nuclear Reactions, Joint Institute for Nuclear Research, Dubna, Russia*

Received 23 June 1997; revised 16 July 1997; accepted 30 July 1997

Abstract

The spectrum of neutrons emitted after the β-decay of ^{11}Li has been measured with a large time-of-flight array. The spectrum exhibits six peaks corresponding to neutron emission from known states in the ^{11}Be daughter nucleus. The measured branching ratios indicate significant feeding to states over a broad energy range. The energies and parities of the states are in very good agreement with the previous results of the ^{9}Be(t,p) reaction. Comparison of the present results with shell model calculations indicate the effect of the two neutron halo in ^{11}Li. The beta-delayed neutron spectrum of ^{8}He was determined in order to remove contributions from beam contamination. © 1997 Elsevier Science B.V.

PACS: 27.20.+n, 23.40.-s

[1] Present Address: Department of Chemistry, Indiana University, Bloomington, IN-47405, USA.
[2] Permanent Address: LPC-ISMRA, Boulevard du Marechal Juin, 14050 Caen Cedex, France.
[3] Present Address: Department of Chemistry, Oregon State University, Corvallis, OR 97331, USA.
[4] Permanent Address: Department of Physics and Astronomy, Mississippi State University, Mississippi State, MS 39762, USA.
[5] Permanent Address: Department of Chemistry and Cyclotron Institute, Texas A & M University, College Station, TX 77843, USA.
[6] Permanent Address: Canberra Industries, 800 Research Parkway, Meriden, CT 06450-7122, USA.

PII S0375-9474(97)00410-7

1. Introduction

The heaviest lithium nucleus, ^{11}Li, has been extensively studied and yet continues to hold the attention of many scientists. Attention originally focused on ^{11}Li because this nucleus has many intriguing decay properties [1–8]. For example, a very large number of beta-delayed decay channels are open due to the large beta-decay Q-value (20.7 MeV) [9]. More importantly, ^{11}Li has a very low two-neutron separation energy and has an unusually large breakup cross section [10] that have lead to the description of ^{11}Li as a ^{9}Li core plus two valence neutrons with a very extended spatial distribution [11]. A large number of theories have been advanced to explain the large reaction cross section but the basic structure of this nucleus and its (few) nearest neighbors remain uncertain. Thus, the present determination of the beta-decay branching ratios provides new and important information on the structure of ^{11}Li.

Another intriguing aspect of the beta-decay of drip-line nuclei is that super-allowed transitions have been identified in the heaviest low-Z nuclei that may be linked to neutron-halo structures [12,13]. A recent theoretical analysis has shown the effect of the unusual structures of the ^{11}Li and ^{11}Be states on the beta-decay transition strengths [14]. Because of the poor overlap between the halo parent state and the normal daughter states, one might expect poor agreement with shell model calculations of the ^{11}Li decay modes if the neutron halo is not well represented by harmonic oscillator wavefunctions or has large admixtures of states outside the model space.

The basic decay modes of ^{11}Li were established almost twenty years ago [2] and during the intervening period a large effort has been made to establish the branches to the many open channels, some of which are quite exotic. As an example, the complete disintegration of the daughter ^{11}Be nucleus into two alpha particles plus three neutrons has been observed [6]. Also, the energies of low-lying states in the daughter nucleus ^{11}Be have been remeasured with the ^{9}Be(t,p) reaction and a detailed analysis of their shell model configurations has been made [15]. More recently, beta-delayed deuteron emission has been observed [16], the branching ratio to the single bound state in ^{11}Be has been remeasured [17], and there has been a preliminary report of beta-delayed-neutron gamma-ray coincidence study [18].

Single neutron emission following beta decay occurs with a probability of $87.6 \pm 0.8\%$ [17]. Although measurements have been made of the lowest energy portion of the neutron spectrum with ^{3}He filled proportional counters [2], the feeding of a few of the states in the ^{11}Be daughter is only known by inference. Here we report a direct, high resolution measurement of the energy spectrum of beta-delayed neutrons from ^{11}Li by a measurement of their time of flight with a large array of plastic scintillators using a technique that we have applied to a number of light nuclei. Thus, the present experiment is very similar in design and detail to the measurements of beta-delayed neutrons carried out recently by Harkewicz et al. [19] and Scheller et al. [20]. The analysis presented in this report concentrates on the measurement of the distribution of single neutrons following the β-decay of ^{11}Li. In addition to ^{11}Li, separate measurements of the beta-delayed neutrons from ^{17}N were used to calibrate the array and the beta-delayed neutrons

from ^{8}He were measured to subtract a background contribution from this impurity in the beam of secondary ions.

2. Experimental

The experiment can be summarized as follows: a sample of radioactive ions were created in a projectile fragmentation reaction, separated by the A1200 projectile-fragment separator, and implanted into a plastic scintillator. After a short collection time the beam was turned off. At this point, the coincident neutrons were detected in a large array triggered by the beta-particle and the times of flight were measured on an event-by-event basis. This process was repeated automatically over a period of several days.

The nuclei to be studied were produced by fragmenting an E/A = 80 MeV ^{18}O beam from the K1200 cyclotron at the National Superconducting Cyclotron Laboratory (NSCL) in a 790 mg/cm^2 beryllium metal target. The typical ion current was ~25 particle nA. The A1200 fragment separator at the NSCL was operated in the momentum-loss achromatic mode to separate the ions to be studied from the many other projectile residues [21]. The A1200 utilizes an initial magnetic analysis (to select all products with m/q values within approximately ±1.5% of a given value) followed by passage through a momentum-loss foil (introducing a Z-dependent shift breaking m/q ambiguities) and a second magnetic analysis to select and focus individual products. In the present study, the momentum-loss degrader was a carbon foil, ≈710 mg/cm^2 thick. During the main experiment, the production rate was approximately 20 ^{11}Li ions/(spnA). Separators like the A1200 produce ion beams with contaminants that are close (typically ±1 unit in Z or N) to the selected fragment. The secondary beam also contained ^{8}He ions at the level of ~5%. Near the end of the experiment, a small amount of time was used to implant and remeasure [22] the beta-delayed neutron spectrum of ^{8}He with this apparatus. At the beginning of the experiment a beam of ^{17}N was produced and delivered to the neutron array for calibration purposes.

The beams of radioactive ions were transported to an experimental vault that was approximately 30 m from the A1200 focal plane and a total of 49 m from the production target, with intervening shielding walls. As a result, the ambient neutron background at the site of the measurement was very low. In this remote vault, the energetic beam of radioactive ions passed through a vacuum window and into the air. After approximately 1 m, the ions encountered an energy degrader (whose thickness was adjustable), a silicon surface barrier detector, (SSB, 200 μm thick), and then came to rest in a plastic scintillator (1 cm thick) connected to two photomultiplier tubes. The number and isotopic identity of the implanted ions was thus continuously measured during the entire experiment by the combination of energy-loss in the SSB and time-of-flight versus the phase of the cyclotron radio-frequency accelerating voltage. A second SSB detector was placed after the plastic scintillator to insure that the isotope of interest did, in fact, stop in the plastic scintillator.

The implantation detector was surrounded by an array of sixteen plastic scintillators

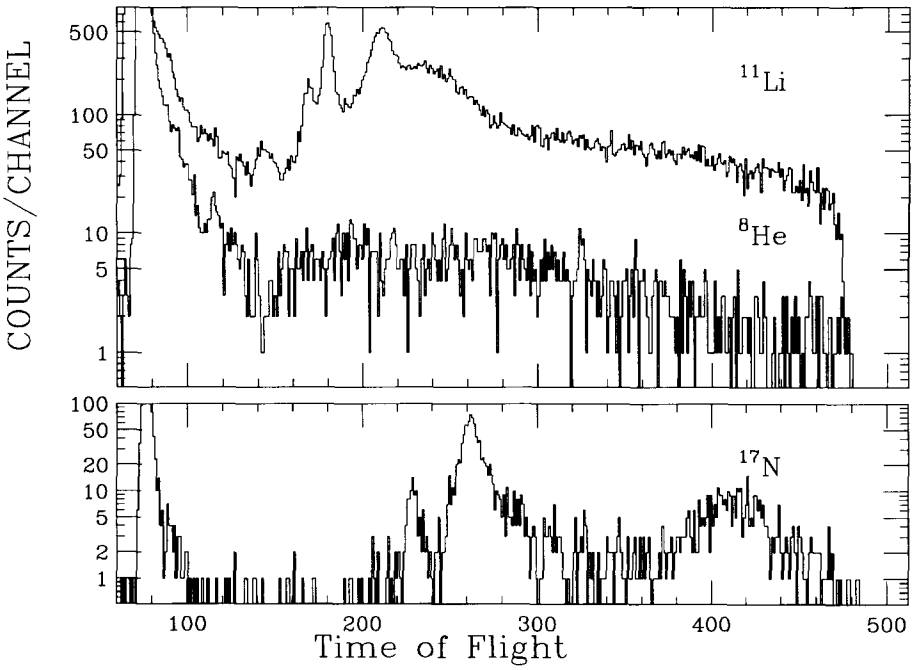

Fig. 1. The time of flight distributions for a single neutron array element (#2) from each of the nuclei in the present study. The ordinate is channel numbers with a calibration of 343.3 ps per channel.

that had a radius of curvature of 1.00 m, described previously [19,20]. These scintillators were sensitive to beta particles and neutrons. The mean time of arrival relative to the mean start signal from the implantation detector was used to determine the velocity and thus the energy of each neutron. During the fixed beam-off time interval, beta-decay of the implanted ions triggered a system to record the relative times of flight (TOF) of particles detected in the plastic scintillators. The TOF spectra obtained during part of the experiment in a typical element of the neutron array for each of the implanted ions are shown in Fig. 1.

The efficiency and the energy calibration of the neutron array was obtained for each array element by normalizing the results of a Monte Carlo calculation to the measured efficiency for beta-delayed neutrons from the three states in ^{17}N as described by Scheller [20]. The intrinsic neutron efficiency of each array element peaked at approximately 22% at 1 MeV and was a slowly decreasing function of energy at higher energies. The uncertainty in the efficiency calibration was approximately 6% and dominated the statistical uncertainties. Some effort was made to enhance the detector efficiency for low-energy neutrons relative to the earlier measurements. The 0.383 MeV neutrons from ^{17}N were observed in all except one array element, see for example, Fig. 1.

The ion-production was cycled *on* and *off* according to a fixed clock attached to a phase shifter in the cyclotron rf-system that could change the relative phase of one of the resonators in the cyclotron by a few degrees. The acceleration of the beam is disrupted by such a shift and the fragment production stops. Most of the data for ^{11}Li

Table 1
The γ ray intensities in percent following ^{11}Li β decay

E_γ (keV)	this work	Ref. [17]	Ref. [18]	Ref. [5]	Ref. [3]
219	0.78(6)	0.55(10)	0.5	0.95(35)	–
320	7.8(8)	6.3(6)	7.6(8)	5.2(14)	9.2(7)
2590	6(1)	8.0(12)	8.5	3.5(10)	–
2811	2.8(3)	0.8(2)	1.0	1.6(7)	–
3368	33(3)	29(3)	33.3	21(6)	35(3)

were collected with a cycle in which the beam was *on* for 25 ms and *off* for 25 ms. Some data was obtained with cycle times of 25 ms *on* and 50 ms *off*.

An unshielded intrinsic germanium detector was also placed near the implantation detector at an angle of approximately 135°. Beta-delayed gamma rays in coincidence with the implantation detector were measured by this detector for comparison to previous work. The efficiency of the detector was measured after the experiment with calibrated sources of ^{152}Eu, ^{60}Co and ^{137}Cs placed at the position of the implantation detector.

3. Results

The time distributions of: (a) events in the trigger detector only, (b) of all particles detected in the array, (c) of relativistic β particles detected in the array, and (d) β-neutron coincidences were analyzed separately. All the distributions were dominated by a single component but the time distribution of the inclusive events included a longer-lived component not present in coincidence with neutrons. The long lived beta emission comes from the equilibration of the ^{11}Be daughter ($T_{1/2}$ = 13.8 s) in the implantation detector that is not a delayed neutron emitter. A small correction for the computer deadtime of 250 μs/event was applied to the data. The neutron coincidence data were then fitted with a single component exponential curve plus a constant background using a chi-squared minimization technique. The resulting half-life for ^{11}Li of 8.99 ± 0.10 ms is in excellent agreement with the value of 8.83 ± 0.12 ms reported by Björnstad et al. [5].

The γ rays following the decay of ^{11}Li have been studied extensively, see Björnstad et al. [5] and references therein, and also more recently by Borge et al. [17]. The γ ray spectrum observed in coincidence with beta-particles in the present work is shown in Fig. 2 and compared to earlier work in Table 1. The spectrum contains a large number of lines from room background but the new results are in good overall agreement with the recent work which were slightly different from the values reported earlier. For example, the 320 keV line from the first excited state in ^{11}Be was found to be present with a $7.8 \pm 0.8\%$ branch. The recent measurements of the branch to the first excited state was $6.3 \pm 0.6\%$ [17], whereas the earlier work gave $5.2 \pm 1.4\%$ [5] and $9.2 \pm 0.7\%$ [3]. Too few β–γ–neutron triple coincidences were observed in the present work to be useful.

The ^{8}He impurity in the radioactive-ion beam was an additional source of "back-

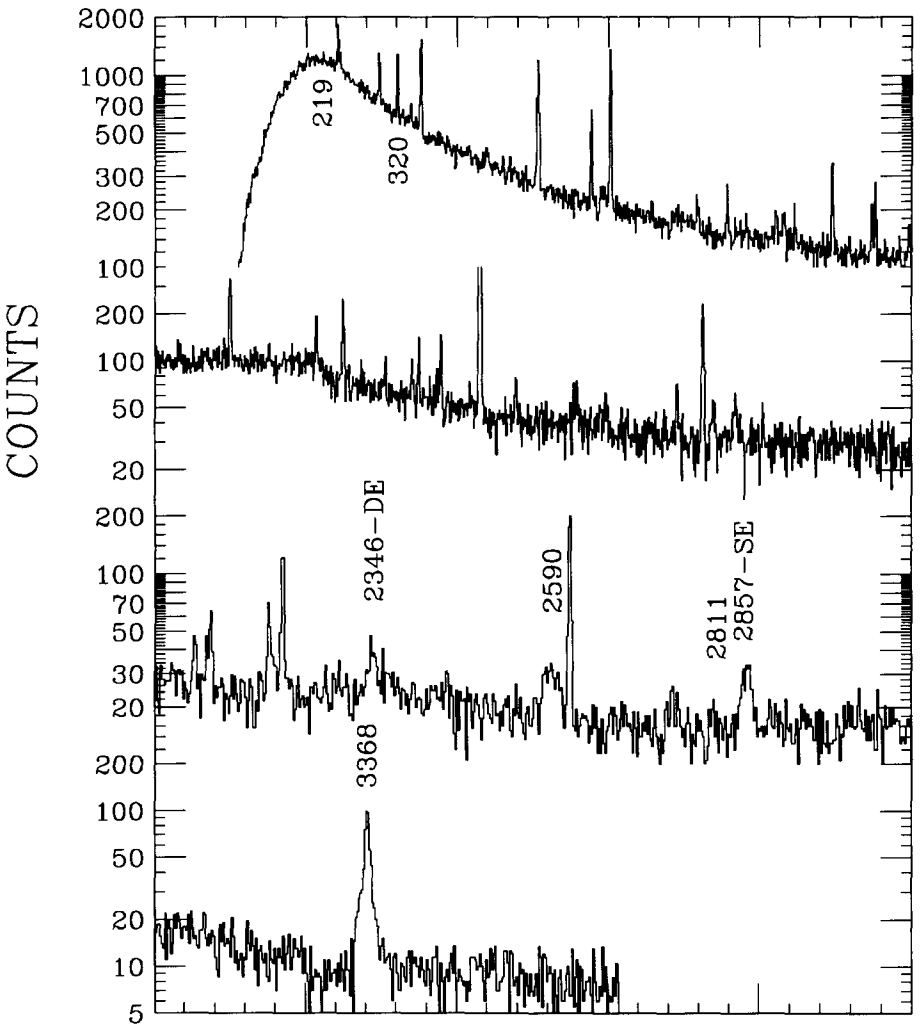

Fig. 2. The gamma ray spectrum observed in coincidence with beta rays following the implantation of ^{11}Li. The spectrum is shown in four segments, 1000 channels each, with an energy calibration of approximately 1.029 keV/channel. The transitions listed in Table I are labeled by their energy in keV.

ground" neutrons. The beta-delayed neutron probability from ^{8}He is known to be small ($16 \pm 1\%$) but the shape of the spectrum is not so well known [22,23]. Therefore, a small amount of time was used to deliver a beam of ^{8}He to the array and measure this beta-delayed neutron spectrum. The TOF spectra were generally featureless, see for example Fig. 1. The calculated energy distribution of neutrons following ^{8}He decay, shown in Fig. 4, was found to be very broad with two shoulders corresponding to the emission of neutrons from the broad states at 3.21 and 8.8 MeV in the ^{8}Li daughter. The contribution from ^{8}He decay, normalized to the number of ^{8}He ions implanted during the ^{11}Li study, was subtracted from each individual array spectrum prior to analysis.

The neutron spectra from the detector array were fitted in the TOF domain and one

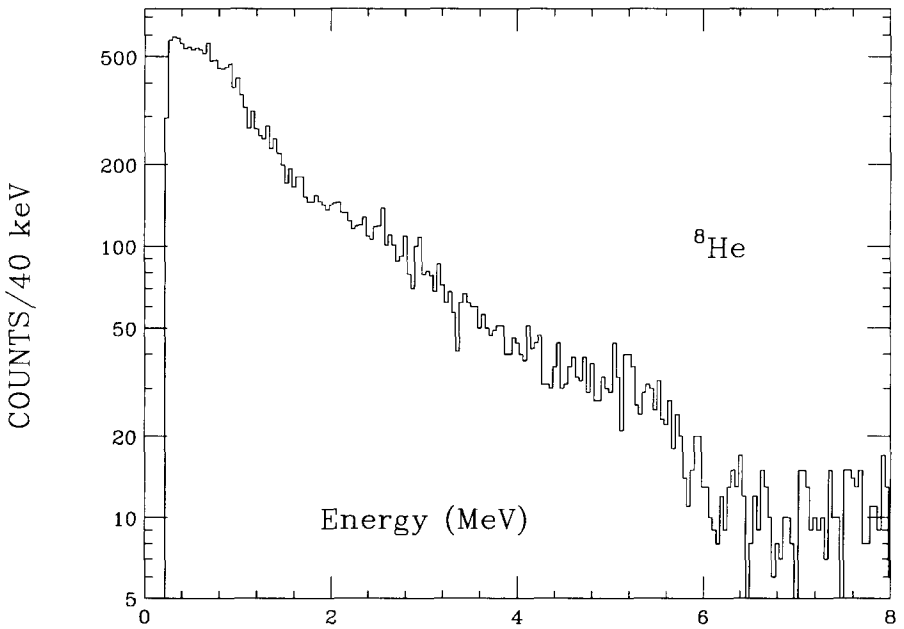

Fig. 3. The calculated energy spectrum in MeV of neutrons following the beta-decay of ^{8}He decay uncorrected for detector efficiency. The data from all the array elements were added together to obtain this figure.

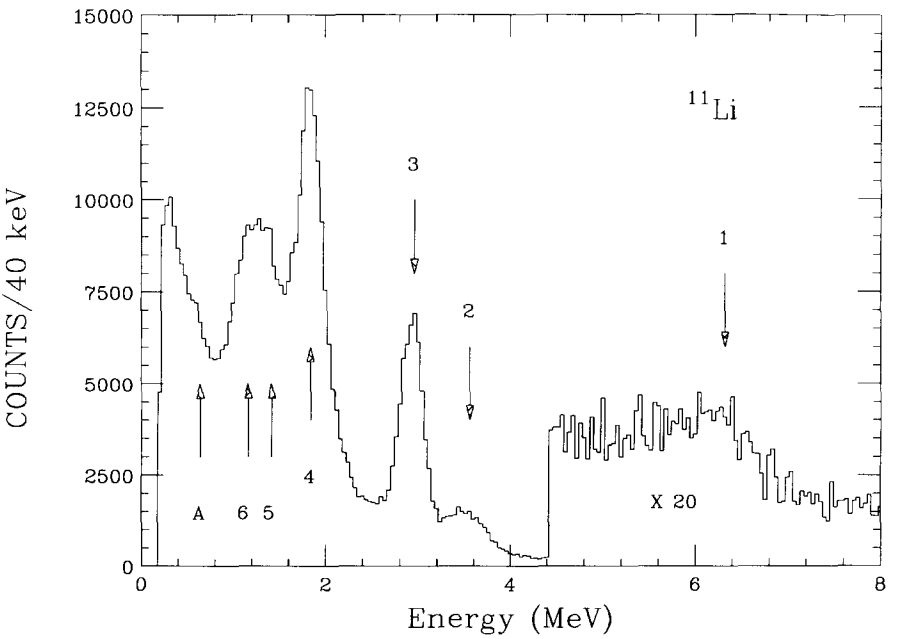

Fig. 4. The calculated energy spectrum in MeV of all single neutrons following the beta-decay of ^{11}Li decay uncorrected for detector efficiency.

Table 2
Summary of the measured and inferred feeding of the states in ^{11}Be

Energy level	Measured			Reference
literature (keV)	energy (keV)	branch (%)	$B(GT)$ [a]	or note
g.s.		<2.		Ref. [4]
0.320	0.320	7.8(8)	0.0084(9)	this work
		6.3(6)	0.0068(7)	Ref. [17]
		7.6(8)	0.0082(9)	Ref. [18]
1.748				
2.642	2.643	33.3(20)	0.064(4)	
3.398				
3.888	3.866	$16.4(10)+x$	0.045(3)	[b]
3.955		$\sim 7.5-x$	0.021(3)	[b]
5.255	5.15	4.9(5)	0.020(2)	
5.849	5.75	10(1)	0.050(5)	
6.51,6.70,7.03		~9	0.060(7)	[c]
8.816		~4	0.058(7)	[d]
10.6	10.92,10.72	6.3(7)	0.199(22)	[e]
18.1		0.30(5)	1.7(2)	Ref. 5,6
		$\geqslant 0.35$	$\geqslant 1.6$	Ref. 13

[a] Calculated as $ft = 6177/[(g_A/g_V)^2 B(GT) + B(F)]$, where $(g_A/g_V)^2 = 1.59$.
[b] To be consistent with gamma ray intensities, branching to the 3.887 and 3.956 MeV states share an additional ~7.5% as described in the text.
[c] Similar to b, branching to these states should total approximately 9% and lead by neutron emission to the states near 6 MeV in ^{10}Be.
[d] The branch to this state is approximately 4% and leads to two neutron emission.
[e] The energy of the state obtained from the neutron transitions 1 and 2, respectively.

summed spectrum was also fitted in the energy domain. Features of the spectrum with higher energies are more distinct in the TOF domain whereas lower energy features are more distinct in the energy domain. A typical measured TOF spectrum can be seen in Fig. 1 and the calculated energy spectrum from the TOF of all detectors is shown at the top of Fig. 4. The ^{8}He-subtracted TOF-spectrum from each detector was individually fitted in order to maintain the maximum resolution. The weighted averages of the sixteen sets of results were used and were very consistent with the independent analysis of the peaks in the calculated neutron energy spectrum. The results are summarized in Table 2 and shown schematically in Fig. 5.

The energy spectrum is quite dramatic as it is made up from six different neutron groups, labeled in the figure and table in decreasing energy order. On the other hand, a small bump, labeled A, inferred from previous observations of charged particles [7] seems to be present at low energies. The measurement by Azuma et al. [2] of the neutron energy spectrum with ^{3}He proportional counters also indicated two additional peaks at very low energies (18 and 80 keV) that were well below the threshold of the present study and were not observed. Unfortunately, the intensities of these low very energy transitions were not reported. The shape of the neutron TOF spectrum agrees

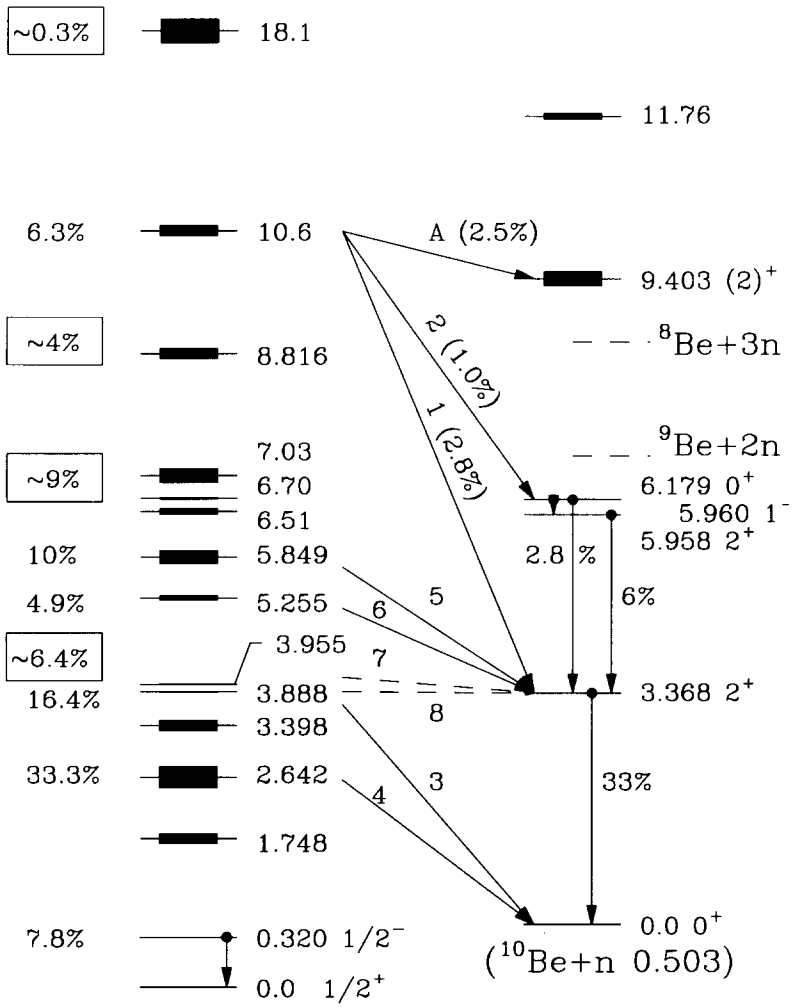

Fig. 5. A schematic diagram of the neutron and γ ray transitions. At the left, the beta-decay branching ratios to energy levels in ^{11}Be, values in boxes were inferred from this and other work are given and at the far right, the energy levels in the neutron decay daughter, ^{10}Be are given. The energies of the states from the literature are given in MeV and their widths are qualitatively indicated by the line thicknesses, known spins and parities are also indicated.

excellently with the preliminary report by Aoi et al. [18] and the energies of the six observed neutrons match well with the energies of the states identified in the ^{9}Be(t,p) reaction studied by Liu and Fortune [15].

The intensities of these neutron transitions were combined with the known neutron multiplicities [5,17] and the measured γ-ray transitions to construct the beta-decay feeding of states in ^{11}Be. For example, the difference between the observed neutron branches to the 3.368, 2+ state in ^{10}Be and the γ-ray intensity emanating from this state is approximately 7.5%. This unobserved neutron strength should be divided between the very low energy neutron transitions numbered 7 and 8, not observed in the present

study. Aoi et al. indicated a the somewhat lower value of 10% for transition #7 and transition #8 was similarly below their detection threshold. The feeding of the levels near 6.5 MeV in ^{11}Be followed by neutron emission must be approximately 9% to account for the γ ray transitions from the levels near 6 MeV in ^{10}Be. The very low energy neutron transitions from the 6.51 and 6.71 MeV states in ^{11}Be to the 5.958 and 6.179 MeV states in ^{10}Be would not be observed in the present work. The branch to the 8.816 MeV state in ^{11}Be must be approximately 4% in order to account for the two-neutron emission probability. The branch to the 10.6 MeV state in ^{11}Be is the sum of the high energy neutrons labeled 1 and 2 plus an estimate of the bump labeled "A" in Fig. 5. The estimated area of "A" is $2.5 \pm 0.3\%$, in good agreement with the value of $2.9 \pm 0.65\%$ from Langevin et al. [7]. The total beta-decay intensity to excited states in ^{11}Be is $99.5 \pm 6\%$. Thus, beta-decay to the ground state of ^{11}Be is $0.5 \pm 6\%$, a result which is consistent with the previous estimate of $<2\%$.

It should be noted that Aoi et al. [18] have assigned four neutron transitions to a previously unknown state in ^{11}Be at 8.03 MeV and have not included significant feeding of the 18 keV neutron from the 3.882 MeV state in ^{11}Be. The assignments made in the present work include the low energy neutron and do not require a new state. The analysis of the doppler-broadened peak shape of the 3368 keV transition in ^{10}Be described by Borge et al. [17] may help resolve this difference.

Overall, the beta-decay of ^{11}Li feeds a number of states over a large energy region. With the exception of the 18.1 MeV state, the calculated log ft values are in the range of 5.67 (0.320 MeV state) to 4.29 (10.6 MeV state) and are consistent with the log ft values of allowed transitions. For such allowed transitions, the populated states in the daughter should have negative parities and the unpopulated states should have positive parities. These parity assignments agree exactly with the (t,p) results with the sole exception that the reported parities of the 3.41 and 3.89 MeV states be reversed (cf. Table. 3 in Ref. [15]). Note that the small branch to the 18.1 MeV state was inferred from the charged particle work originally gave a log ft value of 3.4 ± 0.4 that is indicative of a super-allowed decay, as discussed previously [12]. The feeding has been remeasured recently giving a $B(\mathrm{GT}) \geqslant 1.6$ [13] and no evidence was found for significant neutron emission from this state.

4. Discussion

The structures of both ^{11}Li and its daughter ^{11}Be have been intensively studied. The shell model has been very successful in predicting a wide range of nuclear properties of the p-shell nuclei and these nuclei represent a challenge because they are so neutron-rich. The distribution of beta-decay strength observed in the present study provides some new insight into their structure.

Suzuki and Otsuka have calculated the effect of the neutron halo on the Gamow–Teller (GT) transition strength to the 0.320 MeV 3/2- level in ^{11}Be [14]. First, we should note that the log ft value from recent work is slightly larger than the older value

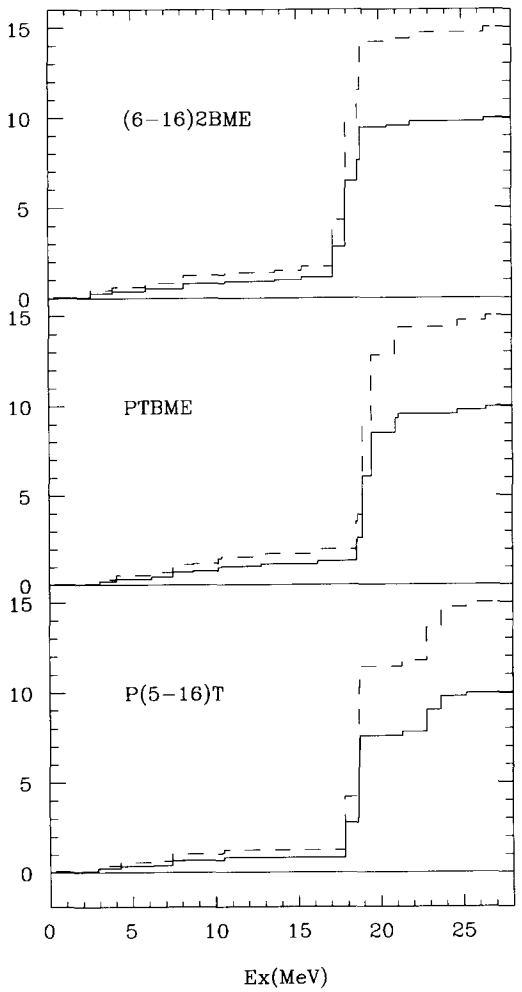

Fig. 6. Total GT strength obtained with the three 0p-shell interactions discussed in the text. The strength is shown as a running sum of the excitation energy. The dashed line is with the free-nucleon GT operator and the solid line is with the effective (renormalized) GT operator.

in the literature and that the probability of $\nu p_{1/2}^2$ character in the ^{11}Li wavefunction determined by Suzuki and Otsuka should be significantly lower [14]. A similar analysis of the admixture was recently described by Borge et al. [17] with their newly measured branching ratio that suggested approximately 50% s-type admixture in the wave function. This particular transition is, however, only 0.06% of the sum rule value, $3(N-Z) = 15$, and is extremely sensitive to all aspects of the calculation, in particular the 0p Hamiltonian. The total transition strength to all low-lying states up to about 10 MeV observed in this experiment is a much less model dependent measure of the neutron halo properties.

We have investigated the β decay properties of ^{11}Li with the conventional 0p shell model [24] and its extension to include effects from "intruder" 1s0d shell configurations.

The 0p model-space allows for all possible mixing between the $0p_{3/2}$ and $0p_{1/2}$ orbital configurations. The summed β^- $B(GT)$ values for the ^{11}Li to ^{11}Be decay are shown as a function of excitation energy in Fig. 6. The calculations were performed with three different effective interactions using the free-nucleon Gamow–Teller operator (dashed lines) and an effective operator (solid lines). Since the β^+ strength is zero in the 0p shell model, the sum rule of $3(N - Z) = 15$ applies to the β^- strength and to all calculations. As observed in the 1s0d shell [25], the experimental GT strengths of 0p shell nuclei are systematically reduced (quenched) relative to the free-nucleon operator calculations. The matrix elements obtained from the effective operator obtained from a fit to experiment (the operator from the bottom left of Table 4 in Ref. [26]) are lower than the free-nucleon values by a factor of about 0.815, and the GT strength is reduced by a factor of about 0.66. The sum rule is, therefore, reduced to about 10.0. This reduction is due to higher-order nucleon configuration mixing (beyond the 0p shell) and delta admixtures [27].

We have chosen three representative 0p shell interactions that have been obtained from analyses of global 0p-shell energy-level data. The top panel of Fig. 6 indicates the results with the $(6 - 16)$2BME interaction obtained by Cohen and Kurath [28] in a least squares fit of two-body Hamiltonian matrix elements to the energy-level data that was available in 1965. More recent 0p-shell energy-level data was used in the two-body matrix-element fit of Julies, Richter and Brown [29] and the GT distribution obtained with this interaction (PTBME) is shown in the middle panel of Fig. 6. Finally, we show the GT distribution calculated with the $P(5 - 16)T$ interaction [30].

The results from all three calculations show a similar pattern. There are four types of neutron to proton components in the GT decay amplitude: (a) a low-lying $0p_{1/2}$ to $0p_{3/2}$ transition, (b) a medium-energy $0p_{3/2}$ to $0p_{3/2}$ transition, (c) a medium energy $0p_{1/2}$ to $0p_{1/2}$ transition, and (d) a high-energy $0p_{3/2}$ to $0p_{1/2}$ transition. These components mix, resulting in a low-energy region below 15 MeV, where (a) dominates but is partially cancelled by smaller admixtures of (b), (c) and (d), and a narrow giant GT resonance region around 17 MeV in excitation energy where all amplitudes are in phase. The present experiment gives a total strength in the region up to 10 MeV in excitation energy in ^{11}Be which is about a factor of two smaller than theoretical results; compare the dashed and solid line in Fig. 7, respectively.

None of these calculations explicitly takes into account the halo nature of ^{11}Li. Three effects of the halo may be important: (1) Since the $1s_{1/2}$ neutron orbital is the ground state of ^{11}Be, the wavefunction of the last two neutrons in ^{11}Li are expected to have some $(1s0d)^2$ admixture. This component has no overlap with the final state and is another source of reduction. (2) The overall strength of transition components which start with a $0p_{1/2}$ neutron should be reduced since the large radial extent of the $0p_{1/2}$ neutron will have a reduced radial overlap with the more tightly bound 0p protons. (3) The quenching necessary in the calculations described above may be smaller (a factor closer to unity) for the "free" neutrons in the halo. All of these effects of the halo will modify the $0p_{1/2}$ neutron contributions labeled (a) and (c) relative to the $0p_{3/2}$ contributions labeled (b) and (d).

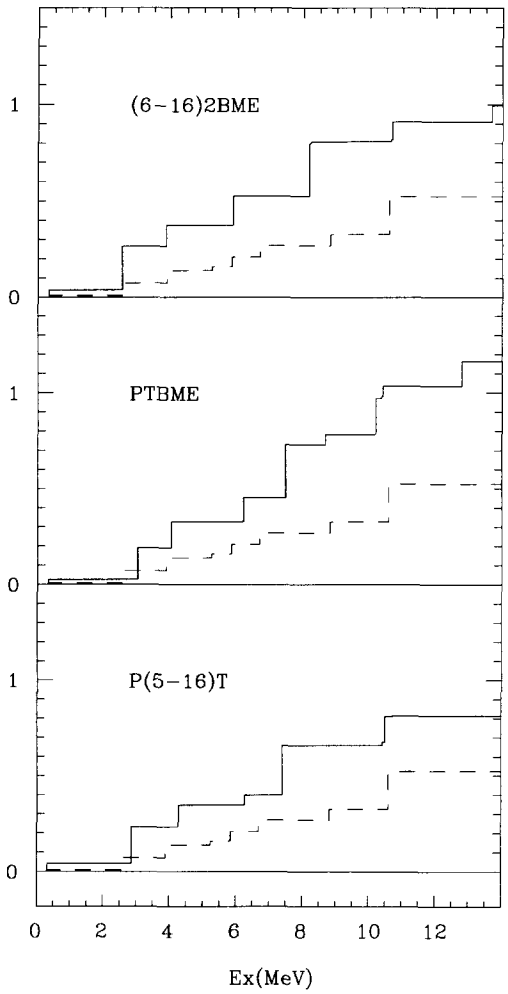

Fig. 7. Low-lying GT strength obtained with the three effective interactions and with the effective GT operator (solid lines) compared to the present experiment (dashed lines).

We explored the distribution of the GT strength when components (a) and (c) were multiplied by an overall factor that ranged between 0.0 and 1.0. The calculations (solid lines) are compared to the data (dashed lines) in Fig. 8. We chose to show this comparison with the Cohen–Kurath (6 – 16)2BME interaction because this interaction gave the best agreement (again with the renormalized operator) for the low-lying decay of ^{9}Li [31] which is the core of the two loosely bound neutrons in ^{11}Li. (The conclusions are similar with the other two interactions.) The variation of the solid lines seen in Fig. 8 is due to the cancellation between the (a) and (b,c,d) components of the transition amplitude. The cancellation is maximized with a reduction factor of about 0.5 below which component (a) begins to dominate. The best agreement is obtained with values of the $0p_{1/2}$ reduction factor, or occupation factor, of either 0.30 or 0.80. Note that the

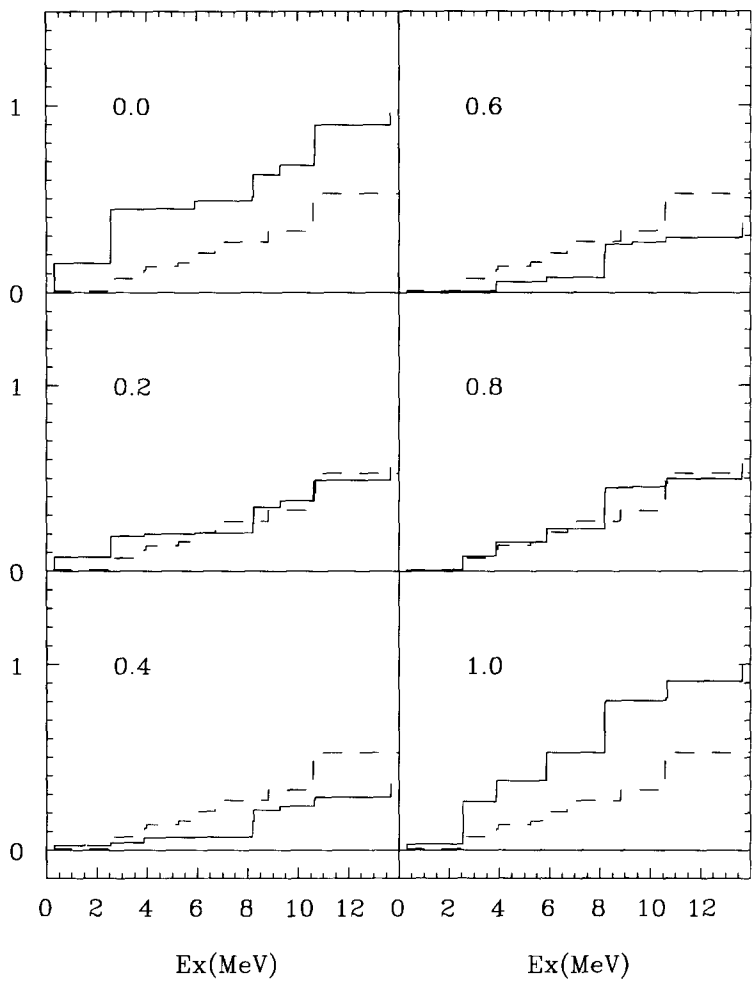

Fig. 8. Low-lying GT strength from the $(6-16)2$BME calculation as a function of the $0p_{1/2}$ reduction factor (solid lines) compared with experiment (dashed lines).

shape of the GT distribution is somewhat better reproduced with the larger value, and we will continue the discussion based upon the larger ($u_e = 0.80$) value.

We would like to arrive at an "empirical" value for the $0p_{1/2}$ occupation number. To do this we should "correct" the empirical occupation factor of $u_e = 0.80$ because the analysis did not include the radial overlap factor and assumed the normal quenching value, the effects labeled (2) and (3) above. Effect (2), the reduction of the radial overlap, can be estimated by using Woods–Saxon wave functions and fixing the binding energy of the valence neutron to be in the range of 0.3 to 0.7 MeV. The calculated neutron $0p_{1/2}$ and proton 0p radial overlap is then 0.81 to 0.85. We thus take this correction factor to be $R_o = 0.83 \pm 0.02$. To account for effect (3), a lower quenching factor for "free" neutrons, we took the simple average value of $R_{q'} = 0.90 \pm 0.10$ between full quenching

(R_q = 0.81) and no quenching ($R_{q''}$ = 1.0) with an uncertainty which encompasses both. Combining the correction factors we arrive at the $0p_{1/2}$ occupation number of: $N(0p_{1/2}) = 2[(u_e R_q)/(R_o R_{q'})]^2 = 1.50^{-0.30}_{+0.40}$. We cannot reduce the uncertainty in this number until the effect of loose binding on the Gamow–Teller quenching is understood.

Shell-model calculations for ^{11}Li have been carried out in a 0+2 $\hbar\omega$ model space [32]. The energies of the lowest unmixed $0\hbar\omega$ and $2\hbar\omega$ $3/2^-$, $T = 5/2$ wavefunctions were found to be nearly degenerate. Mixing these with the "shift method" [33] and the WBT interaction [30] resulted in a wave function for the ^{11}Li ground state which has 54% $0\hbar\omega$ and 46% $2\hbar\omega$ with neutron occupation numbers of 3.69, 1.45, 0.39, 0.7 and 0.39 for the $0p_{3/2}$, $0p_{1/2}$, $0d_{5/2}$, $0d_{3/2}$ and $1s_{1/2}$ orbitals, respectively. (Very similar results were obtained with the WBP [30,34] and WBN[34] interactions.) Note that the calculated $0p_{1/2}$ occupation number is consistent with the empirical value of 1.50 for the $0p_{1/2}$ orbital.

Computationally it is not difficult to calculate the ^{11}Li beta decay directly with 0+2 $\hbar\omega$ wave functions. Although the qualitative properties of the 0+2 $\hbar\omega$ wave functions such as the amount of $2\hbar\omega$ admixture and the occupation numbers are probably reasonable, the detailed properties of the 0+2 $\hbar\omega$ wave functions needed for the β decay calculations are less accurate than the $0\hbar\omega$ 0p shell wave functions. The reason for this lower accuracy is that the 0p part of the WBT interaction has been adjusted within the $0\hbar\omega$ model space and already includes the implicit effects of the $2\hbar\omega$ admixtures. After the $2\hbar\omega$ admixtures are explicitly put in the 0p shell interaction should be modified to account for the double counting. This modification may be particularly important for the very weak GT matrix elements to the low-lying states in ^{11}Be. Thus, 0+2 $\hbar\omega$ calculations with the WBT interaction are probably not reliable, and we believe the analysis presented above is preferable and the best one can do at present. It is important to obtain a new effective interaction within the 0+2 $\hbar\omega$ model space in order to improve upon our analysis. One result that would come out of such $(0+2)\hbar\omega$ calculations that is not present in our 0p-shell calculations is the contribution of the 1s0d-shell orbitals to the Gamow–Teller strength function.

5. Conclusion

In summary, the beta-delayed neutron spectrum of ^{11}Li was determined with a large time-of-flight array. The half-life was found to be in very good agreement with the previous measurement. The intensities of the strong gamma-ray transitions were also found to be consistent with recent work. The delayed neutron spectrum has six strong peaks that indicate emission from levels in the ^{11}Be daughter, plus a weak bump at low energy. Two other very low energy transitions and a low intensity transition at high energy were below the detection thresholds. The neutron intensities were combined with the gamma-ray intensities to produce a consistent and nearly complete picture of the beta-decay feeding of states in the daughter nucleus.

The total transition strength to all low-lying states up to about 10 MeV as observed

in the present experiment provides a less model dependent measure of the neutron halo properties than a comparison of the very small branch to the first excited state in ^{11}Be. The resulting $0p_{1/2}$ neutron occupation number is about 1.5. This value is consistent with a $(0+2)\hbar\omega$ wave function that contains a 54% $0\hbar\omega$ component. In this wave function an average of about one neutron is excited into the 1s0d shell with its occupation about evenly divided between the $1s_{1/2}$ and the $0d_{5/2}$ orbitals. The interpretation of this wave function in terms of the neutron halo properties of ^{11}Li is complicated and depends on the observables under consideration. The total calculated GT strength in the giant resonance region was found to be about 9. It would be interesting to obtain better data for the higher energy region perhaps from inverse reactions with radioactive beams. The position of the IAS is 21.86, 21.13 and 21.31 MeV with the $(6-16)$2BME, PTBME and $P(5-16)T$ interactions, respectively. In all cases the IAS contains the usual $(N-Z)=3$ Fermi strength but only a very little GT strength. Most of the giant GT strength is predicted to lie below the IAS.

Acknowledgements

This work was supported by the National Science Foundation under the grants numbered PHY-92-14992, PHY-95-28844, and PHY-94-03666.

References

[1] E. Roeckl et al., Phys. Rev. C 10 (1974) 1181.
[2] R.E. Azuma et al., Phys. Rev. Lett. 43 (1979) 1652.
[3] C. Détraz et al., J. de Phys. Lett. 41 (1980) 459.
[4] R.E. Azuma et al., Phys. Lett. B 96 (1980) 31.
[5] T. Björnstadt et al., Nucl. Phys. A 359 (1981) 1.
[6] M. Langevin et al., Nucl. Phys. A 366 (1981) 449.
[7] M. Langevin et al., Phys. Lett. B 146 (1984) 176.
[8] K. Riisager et al., Phys. Lett. B 235 (1990) 30.
[9] F. Ajzenberg-Selove, Nucl. Phys. A 506 (1990) 1.
[10] I. Tanihata et al., Phys. Rev. Lett. 55 (1985) 2676.
[11] P.G. Hansen, and B. Jonson, Europhys. Lett. 4 (1987) 409.
[12] M.J.G. Borge et al., Z. Phys. A 340 (1991) 255.
[13] M.J.G. Borge et al., Nucl. Phys. A 613 (1997) 199.
[14] T. Suzuki and T. Otsuka, Phys. Rev. C 50 (1994) R555.
[15] G.-B. Liu and H.T. Fortune, Phys. Rev. C 42 (1990) 167.
[16] I. Mukha et al., Phys. Lett. B367 (1996) 65.
[17] M.J.G. Borge et al., Phys. Rev. C 55 (1997) R8.
[18] N. Aoi et al., Nucl. Phys. A 616 (1997) 181c.
[19] R. Harkewicz et al., Phys. Rev. C 44 (1991) 2365.
[20] K.W. Scheller et al., Phys. Rev., C 49 (1994) 46.
[21] B.M. Sherrill et al., Nucl. Instr. and Meth. B 56/57 (1991) 1106.
[22] T. Björnstadt et al., Nucl. Phys. A 366 (1981) 461.
[23] M.J.G. Borge et al., Nucl. Phys. A 460 (1986) 373.
[24] B.A. Brown and B.H. Wildenthal, Ann. Rev. Nucl. Sci. 38 (1988) 29.
[25] B.A. Brown and B.H. Wildenthal, At. Data Nucl. Data Tables, 33 (1985) 347.
[26] W.T. Chou, E.K. Warburton and B.A. Brown, Phys. Rev. C 47 (1993) 163.

[27] B.A. Brown and B.H. Wildenthal, Nucl. Phys. A 474 (1987) 290.
[28] S. Cohen and D. Kurath, Nucl. Phys. 73 (1965) 1.
[29] R.E. Julies, W.A. Richter and B.A. Brown, South African J. Phys. 15 (1992) 45.
[30] E.K. Warburton and B.A. Brown, Phys. Rev. C 46 (1992) 923.
[31] D. Mikolas et al., Phys. Rev. C 37 (1988) 766.
[32] B.A. Brown, International Conference on Exotic Nuclei and Atomic Masses, Arles, France, June 19–23, 1995 (Editions Frontières, 1995), p. 451.
[33] E.K. Warburton, B.A. Brown and D.J. Millener, Phys. Lett. B 293 (1992) 7.
[34] E.K. Warburton, I.S. Towner and B.A. Brown, Phys. Rev. C 49 (1994) 824.